Int. J. Heat Mass Transfer. Vol. 28, No. 10, pp. 1847–1857, 1985
Printed in Great Britain

0017–9310/85 $3.00 + 0.00

Vertical-channel natural convection spanning between the fully-developed limit and the single-plate boundary-layer limit

E. M. SPARROW and L. F. A. AZEVEDO
Department of Mechanical Engineering, University of Minnesota, Minneapolis, MN 55455, U.S.A.

(*Received* 14 *January* 1985 *and in final form* 1 *April* 1985)

Abstract—The effect of interplate spacing on natural convection in an open-ended vertical channel bounded by an isothermal and an unheated wall was studied both experimentally and computationally. The investigation encompassed the full range of operating conditions of the channel, i.e. from the limit of the fully-developed channel flow to the limit of the single vertical plate. Overall, a 50-fold variation in the spacing between the channel walls was investigated, and the vertical plate was employed in order to achieve the limit of infinite spacing. The experiments were performed in water ($Pr \cong 5$) with the aforementioned parametric variation of the interplate spacing and for an order of magnitude range of the wall-to-ambient temperature difference. The numerical solutions were carried out for the experimentally investigated operating conditions and took account of both natural convection in the channel and conduction in the wall. It was found that the flat plate heat transfer does not form an upper bound for the channel heat transfer. The channel heat transfer is particularly sensitive to changes in interplate spacing for narrow channels and at small temperature differences. The results for all operating conditions were brought tightly together in terms of the groups Nu_s and $(S/H)Ra_s$, and a highly accurate correlation encompassing eight decades of $(S/H)Ra_s$ was developed. Excellent agreement between the experimental results and the computational predictions was obtained.

INTRODUCTION

NATURAL convection is an attractive heat transfer mechanism because of its reliability, simplicity, and cost effectiveness. In particular, natural convection in vertical channels formed by parallel plates is encountered in many applications ranging from the cooling of electronic equipment to the heating of buildings via Trombe walls [1, 2].

The present paper sets forth an experimental and computational study of the heat transfer characteristics of natural convection in an open-ended vertical channel, bounded by an isothermally heated wall and by an unheated wall. The research program was conducted to provide a definitive assessment of the response of the thermal characteristics of the channel to interplate spacing. To this end, experiments encompassing a 50-fold variation of the interplate spacing were carried out. This set of interplate spacings, together with an order of magnitude variation of the wall-to-ambient temperature difference, enabled, for the first time, the investigation of the full range of operating conditions of the one-sided heated channel. This range extends from the fully-developed channel flow regime to the boundary-layer regime for the single vertical plate. Supplementary experiments were also performed for the single vertical plate in order to actually achieve the limit of infinite interplate spacing. The experiments were carried out in water at a nominal Prandtl number equal to 5.

The role of the interplate spacing was highlighted in a presentation in which the heat transfer parameters (Nusselt and Rayleigh numbers) were based on the channel height. Subsequently, the experimental results were rephrased in terms of the more conventional spacing-based parameters, and a correlation was sought which spanned from the fully-developed channel flow regime to the boundary-layer regime for the flat plate.

The conjugate problem consisting of natural convection in the channel and conduction in the unheated wall was solved numerically with the primary objective of verifying that the experimentally determined heat transfer data were not affected by heat conduction in the unheated wall. The numerical results covering the full range of the operating conditions of the experiments were compared with the measured data.

A literature survey revealed only four publications related to natural convection in vertical, open-ended channels bounded by an isothermal and an unheated wall [3–6]. The first of these is a design-oriented study in which correlating expressions were developed for natural convection in vertical channels for several thermal boundary conditions. The procedure utilized in developing these correlations [7] requires expressions for the Nusselt numbers for the limits of very small and very large interplate spacings and experimental data in the intermediate range of spacings. For the thermal boundary conditions of interest here, the latter ingredient (i.e. the data) was not available for the correlation developed in [3]. In particular, the very limited data attributed to [4] (but taken from [6]) displayed considerable scatter. The absence of adequate data made it necessary in [3] to borrow the

NOMENCLATURE

A	surface area of the heated wall
b	thickness of the unheated wall, Fig. 2(b)
C	coefficient in equation (24) with $m = \frac{1}{4}$
F	dimensionless heat flux distribution, equation (16)
G	dimensionless temperature distribution, equation (21)
g	acceleration of gravity
Gr_s	spacing-based Grashof number, $g\beta(T_w - T_\infty)S^3/\nu^2$
H	channel height, Fig. 1
h	average heat transfer coefficient, equation (2)
k	thermal conductivity of water
k_w	thermal conductivity of the unheated wall
Nu_H	height-based Nusselt number, equation (1)
Nu_s	spacing-based Nusselt number, equation (1)
P	dimensionless pressure difference, equation (10)
p	pressure in channel
p_∞	pressure in ambient
p'	pressure difference, $(p - p_\infty)$
Pr	Prandtl number
Q	rate of heat transfer at heated wall
Ra_H	height-based Rayleigh number, equation (3)
Ra_s	spacing-based Rayleigh number, equation (4)
S	interwall spacing, Fig. 1
T	temperature
T_w	temperature of heated wall
T_∞	ambient temperature
$T_{b,e}$	bulk temperature at the channel exit
u, v	velocity components
U, V	dimensionless velocity components, equation (9)
U_0	dimensionless inlet velocity
x, y	coordinates, Fig. 2(a)
X, Y	dimensionless coordinates, equation (8)
W	channel width, Fig. 1.

Greek symbols

β	coefficient of thermal expansion
δ	thermal boundary-layer thickness
θ	dimensionless temperature, equation (10)
λ	transverse coordinate, Fig. 2(b)
Λ	dimensionless transverse coordinate, $\Lambda = \lambda/SGr_s$
ν	kinematic viscosity
ρ	fluid density in the channel
ρ_∞	fluid density in the ambient.

exponent of the correlation from the two-sided heated case. In [5], the main focus was to study pockets of recirculating flow, and heat transfer data were collected only over a small range of interplate spacings.

EXPERIMENTAL APPARATUS AND PROCEDURE

Test section

The test section utilized in the present research was designed with the objective of modeling the geometrical configuration and the thermal boundary conditions described earlier, i.e. a vertical channel of adjustable interwall spacing bounded by one principal wall which is heated and isothermal, and a second principal wall which is unheated. Further, the designed test section should allow the investigation of the vertical flat plate which, as will be demonstrated later, serves as a limiting case.

A pictorial view of the test section is presented in Fig. 1. Its thermally active component was a 0.635-cm-thick copper plate with a height H of 14.52 cm and a width W of 9.67 cm. This plate was electrically heated by three independently controlled heating circuits. Teflon-coated chromel wires (0.00127-cm diameter) were used as the heating elements and were placed in 20 equally-spaced horizontal grooves machined on the back surface of the plate. Since the experiments were to be conducted using water as the working fluid, a water-resistant cement was used to fill the grooves and, thereby, to fix the heating wires. Additionally, two coats of waterproof epoxy paint were applied over the entire rear surface of the plate.

In order to obtain the desired uniform temperature boundary condition at the front surface of the plate, heat was delivered at the rear surface in a nonuniform fashion. The nonuniform heating is reflected in the fact that the lowermost heating circuit encompassed the first four grooves, the middle circuit the next six grooves, and the uppermost circuit the top 10 grooves.

Power was supplied to the heating circuits by a regulated A.C. source. The voltage drop across each heater was carefully adjusted to enable the achievement of uniform wall temperature. This adjustment process was guided by the readings of eight 0.0254-cm chromel–constantan thermocouples installed through the back face of the plate with their junctions located 0.05 cm from the front surface of the plate. The thermocouple wire had been precalibrated to 1 μV. Voltage readings were obtained from a digital voltmeter with an accuracy of

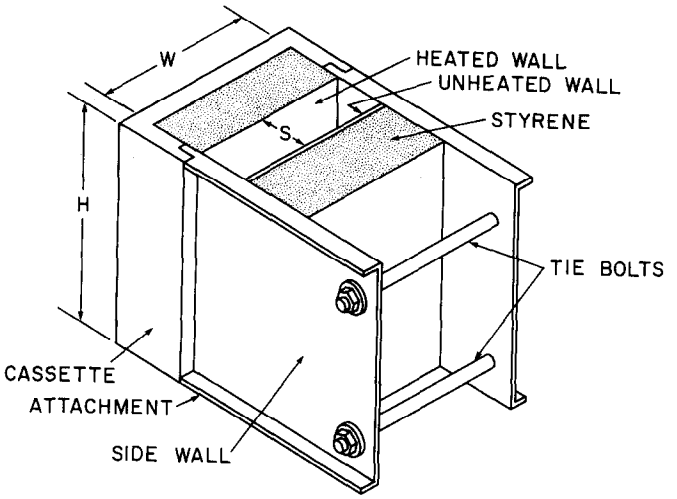

FIG. 1. Pictorial view of the experimental apparatus.

1 μV. The success of the described nonuniform heating layout was attested by the fact that local deviations from the mean plate temperature (i.e. the average of the readings of the eight thermocouples) were always less than 1% of the wall-to-ambient temperature difference.

Backside heat losses were controlled by affixing a 3.2-cm-thick block of closed-pore, water-resistant polystyrene to the rear surface of the plate. The upper and lower edges of the plate were machined in such a way as to allow the polystyrene insulation to cover them. As a result, the front surface was the only part of the plate to directly contact the water.

The C-shaped frame labeled *cassette* in Fig. 1 was a plexiglass structure in which the copper plate and its back-face insulation were housed. As can be noted in the figure, the vertical edges of the C were relieved to enable the cassette to mate with the 0.635-cm-thick plexiglass side walls. Screws were used to bind the mated surfaces together. Attachments were affixed along the upper and lower edges of the side walls to provide symmetric geometries at both the inlet and the exit of the channel.

The other principal wall of the test section, the unheated wall, was made of plexiglass with the same dimensions as the copper plate. Since plexiglass is only a moderately good insulator, a 3.57-cm-thick block of polystyrene was affixed to the back of the plexiglass plate to minimize heat losses.

The interplate spacing S was varied by sliding the unheated wall (i.e. the plexiglass wall with the back insulation) horizontally between the side walls. To set a preselected spacing S, precisely machined spacers were placed between the two principal walls, and the walls were gently pressed together while the two tie bolts were tightened. The spacers were then carefully removed and the spacing verified by a dial-gage-equipped caliper which could resolve 0.0025 cm and better. For the vertical flat plate experiments, the unheated wall and the tie bolts were removed and narrower side walls (2.5 cm in the S direction) put in place.

A plexiglass frame was used to support the test section portrayed in Fig. 1. This frame (not shown in the figure) was designed in such a way as not to obstruct the fluid flow in the vicinity of the channel openings.

Fluid environment

A system of two water-filled chambers, one within the other, was employed as the test environment for the experiments. This particular configuration was chosen with the objective of providing a quiescent ambient, free of extraneously-induced fluid motions for the test section. The heat transfer experiments proper were conducted in the inner chamber. The outer chamber provided thermal control.

The chambers were plexiglass tanks with respective dimensions of $73.1 \times 43.2 \times 45.3$ cm and $101.6 \times 66.0 \times 48.3$ cm (length $\times$ width $\times$ height). The smaller tank, the test chamber, was placed inside the larger tank, resting on three 2.5-cm-high brass bars, so that a water-filled gap existed between the floors of the two tanks. Both the test chamber and the space between the inner and outer tanks (the intertank space) were filled with distilled water. A temperature controller and water circulating unit was installed in the intertank space, providing a highly agitated bath at a preselected temperature that surrounded the test chamber. The outer tank was externally insulated with 2.5-cm-thick styrofoam sheets to further decouple the two-tank system from possible laboratory temperature fluctuations. Heat and water losses due to evaporation were avoided by covering the two tanks with a sheet of styrofoam made impermeable to water by the application of several layers of latex paint. The test section, mounted on its supporting frame, was situated in the test chamber. Three adjusting bolts were provided in the supporting frame so that precise

vertical alignment of the plates could be achieved. The exit of the channel was situated 12.7 cm below the water surface and its inlet at 12.7 cm above the test chamber floor.

Three 0.0254-cm chromel–constantan thermocouples were situated in the test chamber, 30 cm away from the test section. They were mounted on a plexiglass supporting rod and deployed vertically at, respectively, 7.6, 17, and 24 cm above the floor of the test chamber. The thermocouples were used to sense the temperature of the water in the test chamber and to indicate the existence of undesirable temperature stratification within the tank. In all the experiments performed, the maximum deviation from uniformity among the three thermocouples was less than 0.5% of the wall-to-ambient temperature difference.

As will be explained in the description of the experimental procedure, a knowledge of the temperature of the water in the test chamber and in the intertank space was necessary to identify the conditions appropriate for the initiation of a data run. To this end, a 0.1°C ASTM-certified thermometer was installed in each tank.

Experimental procedure

The first step in the experimental procedure for a data run was to set the desired interplate spacing S, as just described. The next step was to verify with the aid of the thermometers that the temperatures of the water in the test chamber and in the intertank space were equal. This equality guaranteed the absence of extraneous, buoyancy-induced fluid motions in the test chamber. If equality did not exist, an overnight waiting period was sufficient to attain the temperature matching.

Next, the voltage settings of the three heating circuits were dialled in. Experience gained from previous runs furnished the relationships among the voltage settings that would yield uniform wall temperature at the heating surface. Power to the heaters was then switched off without, however, altering the voltage settings. The water in the test chamber was manually stirred to eliminate temperature nonuniformities, as sensed by the readings of the three thermocouples. An hour waiting period was allowed after the stirring process to guarantee that motions generated by the stirring operation were no longer present in the test chamber.

Power was then applied to the heating circuits, and the attainment of steady state was monitored by the readings of selected plate thermocouples. At steady state, the readings of the wall and fluid temperatures, voltages, and currents were recorded. Then, a new set of voltages for the next run was dialled in and the power switched off. The stirring of the water in the test chamber was repeated, and a new data run could be conducted after another hour waiting period. The mass of water in the test chamber was such that several data runs could be performed in sequence without altering the temperature equality between the water in the two tanks.

Data reduction

The Nusselt and Rayleigh numbers to be presented in the Results section of this paper were calculated from the experimental data using the procedure that will now be described.

Nusselt numbers, either based on the interplate spacing S or on the plate height H, were calculated by

$$Nu_S = hS/k, \quad Nu_H = hH/k \tag{1}$$

where

$$h = Q/A(T_w - T_\infty). \tag{2}$$

In equation (2), Q is the rate of convective heat transfer to the fluid, and A represents the surface area of the heated plate. Based on a one-dimensional heat conduction model, heat losses through the back of the plate were found to be negligible. Therefore, Q was calculated from the electric power input without any corrections.

The wall temperature T_w was obtained by averaging the readings of the eight plate thermocouples while T_∞, the fluid environment temperature, was computed as the average of the readings of the three thermocouples located in the test chamber. Wall-to-ambient temperature differences ranging from 1 to 10°C were employed during the experiments.

Nusselt number results will be presented as a function of two dimensionless groups, Ra_H and $(S/H)Ra_S$, where

$$Ra_H = [g\beta(T_w - T_\infty)H^3/\nu^2]\,Pr \tag{3}$$

$$Ra_S = [g\beta(T_w - T_\infty)S^3/\nu^2]\,Pr. \tag{4}$$

The thermophysical properties in Nu and Ra were evaluated at the film temperature $\frac{1}{2}(T_w + T_\infty)$.

NUMERICAL ANALYSIS

Numerical solutions were performed to verify that the experimentally determined Nusselt numbers were not affected by conduction in the unheated wall, thereby establishing the generality of the results. The analysis was based on a model consisting of conjugate convection heat transfer in the channel and conduction heat transfer in the unheated wall. In this regard, note that the term *unheated* is meant to indicate the absence of direct heating from an external source. However, the so-called unheated wall may exchange heat with the fluid passing through the channel.

To facilitate the analysis, the problem was divided into two regions as indicated in Figs. 2(a) and (b), which portray, respectively, the convection and the conduction domains. The convection domain [Fig. 2(a)] is characterized by a vertical channel of height H and width S, bounded on one side by an isothermal wall (temperature T_w) and on the other side by a wall whose streamwise temperature and heat flux distributions remain to be determined. The conduction domain [Fig. 2(b)] encompasses the unheated wall whose thickness is b. Aside from the boundary which interfaces with the

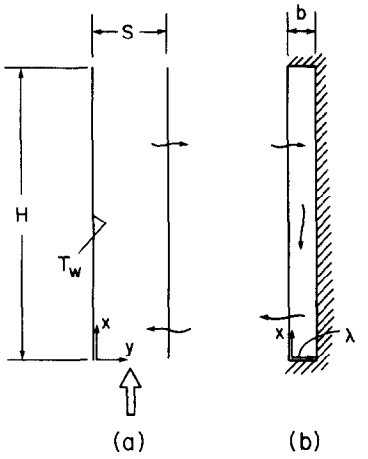

FIG. 2. Convection and conduction domains for numerical solution.

flow, all the boundaries of the conduction domain are locally adiabatic. The arrows in the figure indicate the expected directions of heat flow into, through, and out of the unheated wall.

The temperature and heat flux distributions at the interface of the convection and conduction domains are not known *a priori*. Rather, they are determined as part of the solution of the conjugate problem. An overview of the numerical procedure utilized in the solution will now be given.

The convection problem

The two-dimensional conservation equations governing natural convection in the channel are well documented in the literature and need not be derived here [8]. For the coordinates shown in Fig. 2(a), the dimensionless version of these equations can be written as:

$$\partial U/\partial X + \partial V/\partial Y = 0 \tag{5}$$

$$U(\partial U/\partial X) + V(\partial U/\partial Y) = -\mathrm{d}P/dX + \theta + \partial^2 U/\partial Y^2 \tag{6}$$

$$U(\partial\theta/\partial X) + V(\partial\theta/\partial Y) = (1/Pr)\partial^2\theta/\partial Y^2 \tag{7}$$

where

$$X = (x/S)/Gr_s, \quad Y = y/S \tag{8}$$

$$U = (uS/\nu)Gr_s, \quad V = vS/\nu \tag{9}$$

$$P = p'(x)(S^2/\rho\nu^2)/Gr_s^2, \quad \theta = (T - T_\infty)/(T_w - T_\infty). \tag{10}$$

In the dimensionless expression for the pressure, equation (10), the quantity $p'(x)$ is equal to $p(x) - p_\infty(x)$, which is the imbalance between the pressures within the channel and in the ambient at a given axial location x. The dimensionless channel height is H/SGr_s.

Equations (5)–(7) are to be solved subject to the following hydrodynamic boundary conditions:

$$U = V = 0 \quad \text{at} \quad Y = 0 \quad \text{and} \quad Y = 1 \tag{11}$$

$$U = U_0, \quad V = 0, \quad P = -(1/2)U_0^2 \quad \text{at} \quad X = 0 \tag{12}$$

$$P = 0 \quad \text{at} \quad X = H/S\,Gr_s. \tag{13}$$

The thermal boundary conditions are:

$$\theta = 0 \quad \text{at} \quad X = 0 \tag{14}$$

$$\theta = 1 \quad \text{at} \quad Y = 0 \tag{15}$$

$$\partial\theta/\partial Y = F(X) \quad \text{at} \quad Y = 1 \tag{16}$$

where $F(X)$ is a dimensionless heat flux distribution obtained from the solution of the conduction domain.

For fixed values of the dimensionless height of the channel and of the Prandtl number, there exists only one value of the dimensionless inlet velocity U_0 which yields $P = 0$ at the exit of the channel. In the numerical calculation procedure utilized in the present work, this value of U_0 was obtained iteratively as will be described later.

Once a numerical solution of the governing equations for the channel was obtained, the average Nusselt number for the heated wall was evaluated from

$$Nu_s = hS/k, \quad h = (Q/HW)/(T_w - T_\infty) \tag{17}$$

where Q is the rate of heat transfer from $x = 0$ to $x = H$ at the heated wall.

The conduction problem

The conduction problem in the unheated wall is governed by the two-dimensional Laplace equation, which, in dimensionless form, reads

$$\partial^2\theta/\partial X^2 + \partial^2\theta/\partial\Lambda^2 = 0 \tag{18}$$

where $\Lambda = \lambda/SGr_s$. The boundary conditions for equation (18) are:

$$\partial\theta/\partial\Lambda = 0 \quad \text{at} \quad \Lambda = (b/S)Gr_s = (b/H)(H/S)Gr_s \tag{19}$$

$$\partial\theta/\partial X = 0 \quad \text{at} \quad X = 0 \quad \text{and} \quad X = (H/S)Gr_s \tag{20}$$

$$\theta = G(X) \quad \text{at} \quad \Lambda = 0. \tag{21}$$

The temperature distribution $G(X)$ at the surface of the unheated wall will be obtained from the convection solution.

Convection/conduction matching

The solution of the conjugate problem involved a three-level iteration process, which included a succession of visits with the convection and conduction problems (i.e. the outer iteration) plus iterative solutions for both the conduction and convection problems (i.e. the inner iterations). The two problems were linked through the boundary conditions (16) and (21) at the interface $Y = 1$, $\Lambda = 0$. The outer iteration was initiated by solving the convection problem described by equations (5)–(7) and (11)–(16) assuming $F(X) = 0$ (i.e. locally adiabatic wall). The Patankar–Spalding finite-difference method was used for this task. This scheme is a marching procedure which requires that velocity and temperature be given at $X = 0$. Since the dimensionless height of the channel was fixed, the inlet velocity U_0 at $X = 0$ had to be adjusted until the condition $P = 0$ at the exit of the channel was fulfilled. This was accomplished iteratively utilizing a Newton–Raphson procedure, thereby constituting one of the

aforementioned inner iterations. Once the solution of the convection problem corresponding to $F(X) = 0$ was obtained, the temperature distribution at the unheated wall ($Y = 1$) was recorded and used as the $G(X)$ boundary condition for the conduction problem, equation (21).

A finite-difference method was used to iteratively solve the conduction problem represented by equation (18) with boundary conditions (19)–(21). The heat flux distribution at $\Lambda = 0$ determined from the conduction solution was recorded and transmitted to the convection problem to be used as the $F(X)$ for the next cycle of the outer iteration. Since the heat flux must be continuous across the interface of the conduction and convection domains, $F(X)$ was obtained from

$$F(X) = (k_w/k)(1/Gr_s)(\partial\theta/\partial\Lambda)_{\Lambda=0} \qquad (22)$$

where $(\partial\theta/\partial\Lambda)_{\Lambda=0}$ is from the conduction solution.

The process of transmitting the interfacial $F(X)$ and $G(X)$ distributions between the convection and conduction domains was repeated until the Nusselt number for the heated wall converged to five significant figures. Typically, convergence was achieved with four iterations in the outer loop.

Based on grid dependence tests, the desired numerical accuracy was obtained by utilizing 150×52 and 48×22 grid points (streamwise $\times$ cross stream directions) respectively, in the convection and conduction domains. Due to the difference in the number of streamwise grid points in the two problems, linear interpolation procedures were employed to transfer the $F(X)$ and $G(X)$ distributions between the two domains.

EXPERIMENTAL RESULTS

The response of the experimentally determined channel heat transfer characteristics to variations of the interplate spacing and of the Rayleigh number will now be explored. The investigated range of the interplate spacing was chosen to span between the two limits of fully-developed channel flow and the single flat plate. To this end, 10 interplate spacings, ranging from 1 to 50% of the channel height, were employed. Additionally, to provide results for the limiting case of infinite interwall spacing, experiments were performed for the vertical flat plate. For each interplate spacing and for the vertical flat plate, the Rayleigh number was varied by an order of magnitude by varying the temperature difference between the heated wall and the fluid environment. Experiments were conducted in water at a constant Prandtl number of approximately 5.

The traditional form for presenting heat transfer results for natural convection in channels is to utilize the Nusselt number Nu_s and the dimensionless group $(S/H)\,Ra_s$, both of which are based on the interplate spacing as suggested by theory [8]. This presentation yields excellent correlation of the data as will shortly be demonstrated. This format, however, obscures the role of the interplate spacing. Here, with a view to highlighting the effect of the interplate spacing, the presentation format of Fig. 3 was employed.

In this figure, the Nusselt number Nu_H was plotted against the Rayleigh number Ra_H, both of which are based on the plate height H, which was a constant (= 14.52 cm) for all of the experiments. For a given plate height, Nu_H and Ra_H can be interpreted as, respectively, the dimensionless heat transfer rate and

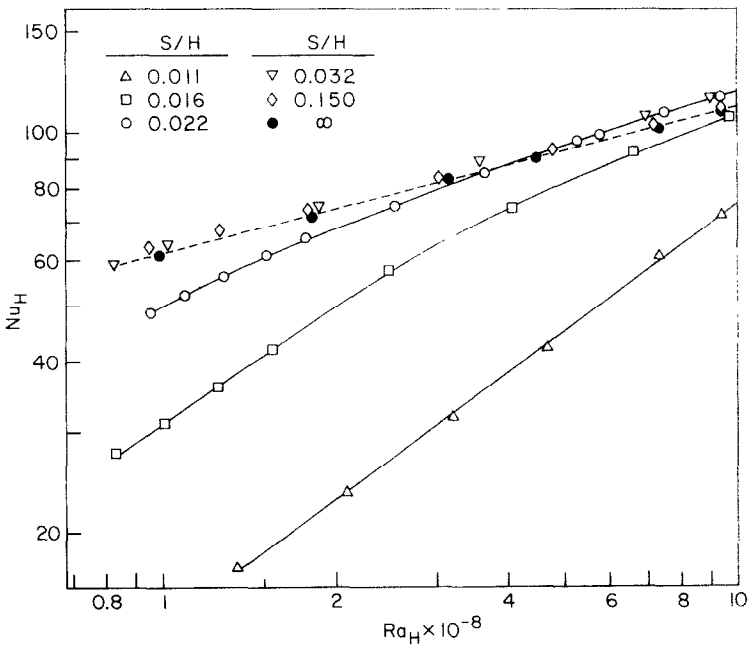

FIG. 3. Experimental height-based Nusselt vs Rayleigh number results for selected S/H in the range 0.011–∞.

the dimensionless plate-to-ambient temperature difference. The dimensionless interplate spacing S/H parameterizes the data as indicated in the legend. To avoid overlap which would create confusion, only selected values of S/H were plotted in Fig. 3 (all the data will be presented shortly). Solid lines were used to interconnect the data for the various $S/H < \infty$, except when they would be too overlapping. In addition, a dashed line based on a least-squares fit was passed through the flat plate data ($S/H = \infty$). The equation of the fitted line is

$$Nu_H = 0.619 Ra_H^{1/4}. \tag{23}$$

It can be noted from the figure that, contrary to the heretofore accepted view [3], the flat plate results do not form the upper bound for the heat transfer rates for the channel. Indeed, there are interplate spacings which produce Nusselt numbers approximately 5% higher than those for the flat plate.

From Fig. 3, a clear picture of the influence of S/H on the heat transfer characteristics of vertical channels emerges. For a given Rayleigh number, there is a range of low S/H where the Nusselt number is highly sensitive to variations of the interplate spacing. At higher S/H, however, the Nusselt number is nearly independent of the spacing. For example, for the lower Rayleigh numbers of Fig. 3, Nu_H is very responsive to interplate spacing for $S/H < 0.022$ (a $3\frac{1}{2}$-fold variation of Nu_H for S/H between 0.011 and 0.022 at $Ra_H = 10^8$). On the other hand, for S/H between 0.032 and ∞, Nu_H varies by only about 5%. At the high Rayleigh number end of the data, the sensitivity of Nu_H to spacing is significantly diminished.

These findings can be rationalized by considering the relative magnitudes of the thermal boundary-layer thickness δ and the interplate spacing S. In particular, there is heightened sensitivity of Nu_H to S/H when the thermal boundary layer spawned by the heated plate spans the interplate spacing, while insensitivity prevails when the thermal boundary-layer thickness is smaller than the spacing. This rationalization is supported by the calculation of the thermal boundary-layer thickness on a flat plate. At $Ra_H = 10^8$, such a calculation yields $\delta/H = 0.0275$ (equation (7.20) of [9]) which, according to Fig. 3, serves admirably as the threshold of significant sensitivity of Nu_H to S/H.

The results for $S/H > 0.032$, which had to be omitted from Fig. 3 due to overlap, are presented in Fig. 4. Overlap is avoided in Fig. 4 by employing individual graphs for each case. In each graph, Nu_H is plotted as a function of Ra_H. The solid lines passing through each set of data are representations of least-squares-based expressions of the form

$$Nu_H = CRa_H^m. \tag{24}$$

It can be seen that the power-law expression provides an excellent representation of all the experimental data of Fig. 4. For comparison purposes, the correlation developed by Churchill and Chu [10] for vertical flat plates is plotted as a dashed line in the lowest graph of

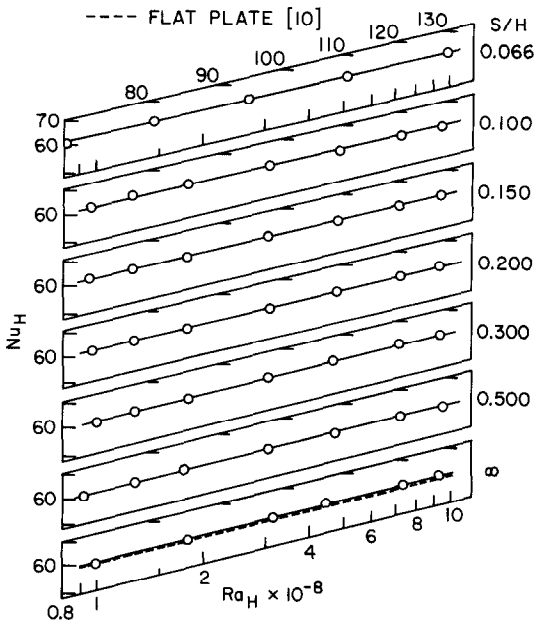

FIG. 4. Experimental height-based Nusselt vs Rayleigh number results for $S/H > 0.032$.

Fig. 4. The maximum deviation between the present flat plate data and the Churchill–Chu correlation (evaluated for $Pr = 5$) is 2.2%. This can be considered a remarkable level of agreement in view of the scatter exhibited by data from different sources presented by Churchill and Chu in Fig. 1 of [10].

The least-squares representations for all of the interplate spacings S/H of Fig. 4 shared the common exponent $m = \frac{1}{4}$. This observation suggests that the coefficient C in equation (24) can be regarded as a measure of the dependence of Nu_H on the dimensionless interplate spacing S/H. In Fig. 5, the coefficient C is plotted as a function of H/S, the reciprocal of the dimensionless interplate spacing. The reciprocal was used to enable the C value for the flat plate ($S/H = \infty$) to be plotted. It should be noted that the ordinate was greatly expanded to improve the resolution of the graph, as indicated by the size of the 1% band shown in the figure.

The magnitude of the coefficient C is seen to decrease toward the flat plate value as the interplate spacing increases (i.e. as H/S decreases). This presentation underscores the point that there is a range of channel interplate spacings which produce Nusselt numbers higher than those obtained with the vertical flat plate. Also, Fig. 5 can be useful for obtaining, via interpolation, C values for interplate spacings other than those investigated here.

The aforementioned differences in thermal performance between the one-sided heated channel and the vertical flat plate will now be made plausible. Vertical channels and vertical plates in natural convection differ fundamentally with regard to the nature of the fluid flow. The flow through a vertical channel is driven by an

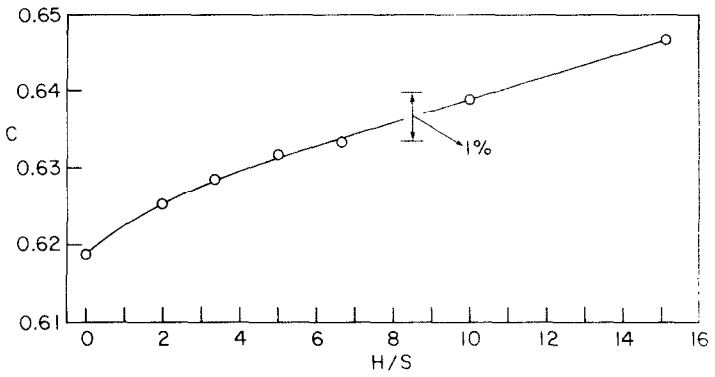

FIG. 5. Dependence of the coefficient C on interplate spacing ($Nu_H = CRa_H^{1/4}$).

imbalance of the hydrostatic pressure drops inside and outside the channel. As far as the channel walls are concerned, the flow entering the channel is a forced convection flow and, as such, should yield higher heat transfer coefficients than those for the flat plate. However, thermal saturation of the fluid passing through the channel can degrade the heat transfer. For the vertical flat plate, thermal saturation does not occur due to the unconstrained growth of the thermal boundary layer.

The thermal saturation effect is most strongly felt by relatively narrow channels, as can be verified in Table 1. In this table, the bulk temperature at the channel exit $T_{b,e}$, presented in terms of $(T_{b,e} - T_\infty)/(T_w - T_\infty)$, is listed as a function of the dimensionless interplate spacing for a fixed value of the Rayleigh number ($Ra_H = 9 \times 10^7$, the lowest investigated Rayleigh number). These bulk temperatures were obtained from the numerical solutions previously described under the assumption that the unheated wall was locally adiabatic. The high levels of saturation $[(T_{b,e} - T_\infty)/(T_w - T_\infty) \sim 1]$ experienced by the channels with small interplate spacing explain the lesser heat transfer performance of these channels compared with the vertical flat plate. For larger values of S/H, the forced convection nature of the channel flow, combined with the now-smaller saturation level, results in Nusselt numbers higher than those for the flat plate.

Table 1. Response of the channel exit temperature to the interplate spacing S/H ($Ra_H = 9 \times 10^7$)

S/H	0.011	0.016	0.022	0.032	0.100	0.500
$\frac{T_{b,e} - T_\infty}{T_w - T_\infty}$	1.00	0.998	0.906	0.649	0.277	0.262

The experimental heat transfer data obtained here will now be presented in Fig. 6 in terms of the Nusselt number Nu_s and of the dimensionless group $(S/H)Ra_s$, which spans eight orders of magnitude. In order to obtain a high degree of resolution of the data while achieving a compact presentation, upper and lower abscissa scales were used as indicated by the arrows.

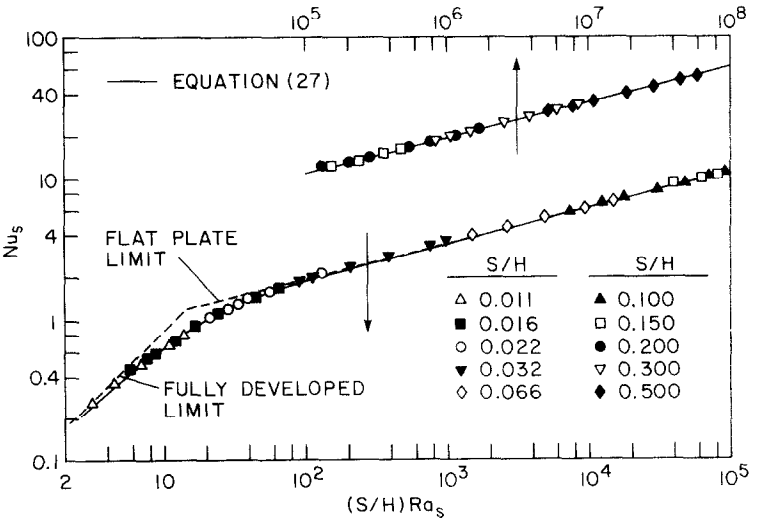

FIG. 6. Experimental spacing-based Nusselt vs Rayleigh number results and their correlation.

The data for the 10 dimensionless interplate spacings are keyed to the symbols identified in the legend.

The most striking feature of the graph is the perfect correlation of the results from all the dimensionless interplate spacings which is achieved by the use of $(S/H)Ra_s$ as the independent variable. For one-sided heated channels, this observation was made previously for a much narrower range of $(S/H)Ra_s$ [5] and is now shown to be valid for $3 < (S/H)Ra_s < 10^8$.

The fact that $(S/H)Ra_s$, a parameter derived from the two-dimensional conservation equations, perfectly correlates the data is an indication that possible three-dimensional effects associated with large values of S/H are not reflected in the Nusselt number Nu_s.

An interpolation formula for Nu_s which spans between small and large $(S/H)Ra_s$ will now be derived based on the method suggested by Churchill and Usagi [7]. This method requires a knowledge of expressions relating Nu_s and $(S/H)Ra_s$ in the limits $(S/H)Ra_s \to 0$ and $\to \infty$ and experimentally determined Nusselt numbers for intermediate values of $(S/H)Ra_s$. In the present work, the expression utilized for $(S/H)Ra_s \to 0$ was

$$Nu_s = (S/H)Ra_s/12 \tag{25}$$

derived in [3] by assuming that fully-developed flow prevailed in the one-sided heated channel. The expression used for the limit $(S/H)Ra_s \to \infty$ is

$$Nu_s = 0.619[(S/H)Ra_s]^{1/4}. \tag{26}$$

This is a rephrased version of the flat plate result, equation (23), to include Nusselt and Rayleigh numbers based on the interplate spacing.

The interpolation relation thus obtained is

$$Nu_s = \{[(S/H)Ra_s/12]^{-n} + [0.619((S/H)Ra_s)^{1/4}]^{-n}\}^{-1/n}. \tag{27}$$

The exponent n was determined to be equal to 2 by comparing equation (27) with the experimental data. Equation (27) is represented in Fig. 6 by the solid line.

The maximum deviation of the experimental data from the values predicted by equation (27) is 6% which, considering the eight-decade range of $(S/H)Ra_s$, is an excellent result.

The dashed lines in Fig. 6 represent the limiting expressions for the Nusselt number, equations (25) and (26).

NUMERICAL RESULTS

In the Numerical Analysis section of this paper, the parameters governing the conjugate problem were identified. They are: the Prandtl number Pr, the Grashof number Gr_s, the dimensionless interplate spacing S/H, the aspect ratio of the unheated wall b/H, and the thermal conductivity ratio k_w/k. The parameters related to the unheated wall were kept constant during the computer runs at the actual values utilized in the experiments, i.e. $k_w/k = 0.28$ (a plexiglass wall in water [11]) and $b/H = 0.044$. For comparison purposes, numerical solutions were also obtained for the channel with the unheated wall being locally adiabatic. All the numerical runs were performed for $Pr = 5$, while $Gr_s = Ra_s/Pr$ and S/H were assigned values which spanned the range encountered in the experiments.

For the entire investigated range of the parameters, the Nusselt number results obtained for the locally adiabatic wall agreed to three significant figures with those for the conjugate problem, which is globally (but not locally) adiabatic. This outcome leads to the conclusion that the unheated wall utilized in the present experiments can be considered, for practical purposes, locally adiabatic and that the Nu_s results obtained are independent of the aspect ratio of the wall and the wall–fluid thermal conductivity ratio.

The numerically determined Nu_s results are plotted as a solid line in Fig. 7 as a function of $(S/H)Ra_s$. Also

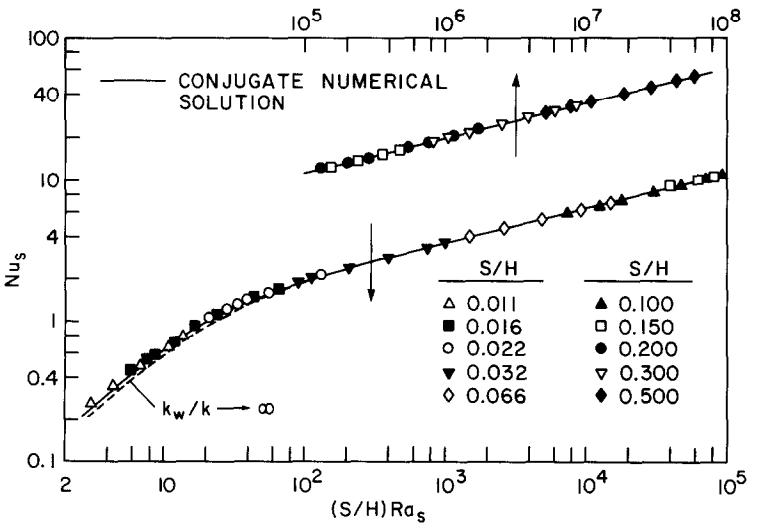

FIG. 7. Comparison of experimentally and numerically determined Nusselt number results.

plotted in the figure are the experimental results previously presented in Fig. 6. It can be seen that the agreement between the experimental data and the numerical results is virtually perfect.

To supplement the numerical work, the influence of the thermal conductivity of the globally-adiabatic unheated wall on the Nusselt number was explored. To this end, the limit $k_w/k \to \infty$ was considered for the unheated wall. If the previously described numerical methodology were to be applied for the $k_w/k \to \infty$ case, convergence problems would arise. The following alternative procedure was devised to overcome this difficulty.

Since the unheated wall is now modeled as being highly conductive, it is reasonable to assume that its temperature is uniform but unknown. For a fixed value of Pr and $(S/H)Ra_s$, there is only one value of the temperature of the unheated wall that will fulfill the globally adiabatic condition, i.e. a value of zero for the surface-integrated heat transfer. This temperature was determined iteratively with the aid of a Newton–Raphson scheme.

The thus-obtained Nusselt number results for the channel with an infinitely conducting unheated wall are plotted in Fig. 7 as a dashed line. It can be seen that for values of $(S/H)Ra_s$ greater than 60, there is no discernible difference between the Nu_s values for the plexiglass-walled conjugate problem and those for $k_w/k \to \infty$. For $(S/H)Ra_s$ less than 60, the deviations are less than 10%.

CONCLUDING REMARKS

The response of the natural convection heat transfer characteristics of a one-sided heated vertical channel to interplate spacing was investigated both experimentally and computationally. The 50-fold variation of the interplate spacing enabled the investigation of all operating conditions between the two limits of fully-developed channel flow and the single vertical plate. Supplementary experiments were also conducted for the latter in order to actually achieve the limit of infinite interplate spacing. For each interplate spacing, the wall-to-ambient temperature difference was varied by an order of magnitude. The experiments were performed in water at a nominal Prandtl number equal to 5.

To highlight the effect of interplate spacing on the heat transfer, the experimental results were first presented in a format in which both the Nusselt and Rayleigh numbers were based on the channel height. This presentation demonstrated that the vertical plate results do not form an upper bound for the channel heat transfer. In particular, channel heat transfer rates were encountered which exceeded those for the flat plate by as much as 5%. Additionally, this presentation facilitated the identification of the regimes of high and low sensitivity of the heat transfer to interplate spacing. Specifically, high sensitivity prevailed for narrow channels and at small wall-to-ambient temperature differences.

The experimental heat transfer data were also presented in terms of the conventional format in which the Nusselt number Nu_s is plotted as a function of $(S/H)Ra_s$. The use of these parameters totally eliminated any separate dependence of the results on S/H over the entire eight-decade range of $(S/H)Ra_s$ that was investigated. This outcome suggests the absence of three-dimensional effects even for relatively large spacings.

A highly accurate representation of the experimental data spanning the fully-developed and flat plate limits was developed in the form

$$Nu_s = \{[(S/H)Ra_s/12]^{-2} + [0.619((S/H)Ra_s)^{1/4}]^{-2}\}^{-1/2} \quad (28)$$

The maximum deviation of the data from this expression was 6%.

Numerical solutions were conducted to verify that the experimentally determined Nusselt numbers were not affected by heat conduction in the unheated wall. To this end, the conjugate problem consisting of natural convection in the channel and heat conduction in the wall was solved by means of finite-difference methods. For comparison purposes, numerical solutions were also obtained assuming the unheated wall to be locally adiabatic. The Nusselt numbers for the conjugate problem agreed to three significant figures with those for the locally adiabatic wall. This finding attests to the independence of the present experimental results from the geometrical and thermal characteristics of the unheated wall. Furthermore, the numerical results displayed virtually perfect agreement with the experiments.

REFERENCES

1. W. Aung, T. J. Kessler and K. I. Beitin, Free convection cooling of electronic systems, *IEEE Trans. Parts, Hybrids Packag.* **PHP-9,** 75–86 (1973).
2. H. Akbari and T. R. Borges, Free convective laminar flow within the Trombe wall channel, *Sol. Energy* **22,** 165–174 (1979).
3. A. Bar-Cohen and W. M. Rohsenow, Thermally optimum spacing of vertical, natural convection cooled, parallel plates, *J. Heat Transfer* **106,** 116–123 (1984).
4. H. Nakamura and T. Shimomatsu, Preprint of the 42nd National Meeting of JSME, paper No. 120 (1964).
5. E. M. Sparrow, G. M. Chrysler and L. F. Azevedo, Observed flow reversals and measured-predicted Nusselt numbers for natural convection in a one-sided heated vertical channel, *J. Heat Transfer* **106,** 325–332 (1984).
6. O. Miyatake and T. Fujii, Free convective heat transfer between vertical plates—one plate is isothermally heated and the other is thermally insulated, *Heat Transfer—Jap. Res.* **1,** 30–38 (1972).
7. S. W. Churchill and R. Usagi, A general expression for the correlation of rates of transfer and other phenomena, *A.I.Ch.E. Jl* **18,** 1121–1128 (1972).
8. J. R. Bodoia and J. F. Osterle, The development of free convection between heated vertical plates, *J. Heat Transfer* **84,** 40–44 (1962).

9. J. P. Holman, *Heat Transfer* (5th edn.), p. 270. McGraw-Hill, New York (1981).
10. S. W. Churchill and H. H. S. Chu, Correlating equations for laminar and turbulent free convection from a vertical plate, *Int. J. Heat Mass Transfer* **18**, 1323–1329 (1975).
11. General Electric Company, Heat transfer and fluid flow data book, New York (1970).

CONVECTION NATURELLE DANS UN CANAL VERTICAL ENTRE LA LIMITE PLEINEMENT ETABLIE ET LA LIMITE DE COUCHE LIMITE SUR PLAQUE UNIQUE

Résumé—On étudie expérimentalement et numériquement l'effet de l'espacement entre plaques sur la convection naturelle dans un canal vertical, ouvert aux extrémités, limité par une paroi isotherme et une autre non chauffée. L'étude concerne le domaine complet des conditions opératoires du canal depuis la limite de l'écoulement pleinement établi jusqu'à la limite de la plaque unique. On peut réaliser une cinquantaine d'espacement entre les parois du canal. Les expériences sont réalisées avec de l'eau ($Pr = 5$) et une différence de température entre plaque et ambiance variant d'un ordre de grandeur. Les solutions numériques sont faites pour les conditions expérimentales et elles prennent en compte la convection naturelle dans le canal et la conduction dans la paroi. On trouve que le transfert thermique à la plaque plane ne forme pas une limite supérieure pour le transfert thermique. Le transfert de canal est particulièrement sensible aux changements d'espacement des parois pour des canaux étroits et des faibles différences de température. Les résultats pour toutes les conditions opératoires sont étroitement rassemblés en terme des groupements Nu_s et $(S/H)\,Ra_s$, et on développe une formule très précise pour huit décades de $(S/H)\,Ra_s$. On obtient un excellent accord entre les résultats expérimentaux et les calculs prévisionnels.

NATÜRLICHE KONVEKTION IM VERTIKALEN KANAL ZWISCHEN DEN GRENZFÄLLEN DER VOLL AUSGEBILDETEN KANALSTRÖMUNG UND DER GRENZSCHICHTSTRÖMUNG AN DER EINZELPLATTE

Zusammenfassung—Der Einfluß des Abstandes auf die natürliche Konvektion zwischen zwei Platten, die einen vertikalen Kanal mit offenen Enden bilden, wurde experimentell und rechnerisch untersucht, wobei die eine Platte isotherm, die andere nicht beheizt war. Die Untersuchung umfaßte den gesamten Bereich der Betriebsbedingungen des Kanals, d.h. vom Grenzfall der voll ausgebildeten Kanalströmung bis zum Grenzfall der einzelnen vertikalen Platte. Untersucht wurde eine fünfzigfache Änderung des Abstandes zwischen den Kanalwänden, eine einzelne vertikale Platte wurde für den Grenzfall des unendlichen Plattenabstandes verwendet. Die Experimente wurden in Wasser ($Pr \approx 5$) mit den zuvor erwähnten Parameterveränderungen des Plattenabstandes und für den Bereich einer Größenordnung für die Temperaturdifferenz von der Wand zur Umgebung durchgeführt. Die rechnerischen Lösungen wurden für die experimentell untersuchten Betriebsbedingungen durchgeführt, wobei die natürliche Konvektion im Kanal und die Wärmeleitung in der Wand berücksichtigt wurden. Es wurde festgestellt, daß die Wärmeübertragung an der ebenen Platte keine obere Grenze für die Wärmeübertragung im Kanal darstellt. Die Wärmeübertragung im Kanal ist besonders empfindlich für Veränderungen des Plattenabstandes bei engen Kanälen und bei kleinen Temperaturdifferenzen. Die Ergebnisse für alle Betriebsbedingungen wurden in Form der Kennzahlen Nu_s und $(S/H)Ra_s$ verdichtet, außerdem wurde eine Korrelation mit hoher Genauigkeit entwickelt, die acht Zehnerpotenzen von $(S/H)Ra_s$ umfaßt. Es wurde eine sehr gute Übereinstimmung zwischen den experimentellen und den rechnerischen Ergebnissen ermittelt.

ЕСТЕСТВЕННАЯ КОНВЕКЦИЯ В ВЕРТИКАЛЬНОМ КАНАЛЕ: ОТ ПОЛНОСТЬЮ РАЗВИТОЙ КОНВЕКЦИИ ДО ПОГРАНИЧНОГО СЛОЯ НА ОДИНОЧНОЙ ПЛАСТИНЕ

Аннотация—Экспериментально и численно изучается влияние расстояния между пластинами на естественную конвекцию в вертикальном канале с открытыми торцами, который ограничен изотермической и ненагреваемой стенкой. Исследование охватывает весь диапазон рабочих режимов канала, т.е. от полностью развитого течения в канале до случая одной вертикальной пластины. В общем, было изучено пятьдесят вариантов расстояний между стенками канала, а вертикальная пластина применялась для моделирования естественной конвекции в безграничном пространстве. Эксперименты проводились в воде ($Pr \cong 5$) для упомянутых выше вариантов изменения расстояния между пластинами и для величины разности температур между стенкой и окружающей средой, лежащей в пределах одного порядка. Численные решения находились для граничных условий, принятых в эксперименте, и при этом учитывались процессы естественной конвекции в канале и теплопроводность в стенке. Найдено, что теплопередача плоской пластины не является верхним предельным случаем для канала. Теплообмен в канале особенно чувствителен к изменению расстояния между пластинами в случае малых разностей температур и узких каналов. Результаты для всех режимов течения были обработаны в переменных Nu_s и $(S/H)Ra_s$, и получены корреляционные зависимости, с большой точностью описывающие данные для 8 декад по переменной $(S/H)Ra_s$. Получено хорошее соответствие между экспериментальными и расчетными данными.